Polarimetric Scattering and Radar Echoes from Inhomogeneous Scatter Media with Rough Interfaces

Ya-Qiu Jin

Key Laboratory of Wave Scattering and Remote Sensing Information (Ministry of Education),
Fudan University, Shanghai 200433, China
Email: yqjin@fudan.ac.cn

Abstract

A theoretical model of stratified lunar regolith media with scatterers and rough interfaces for numerical simulation of polarimetric radar pulse echoes are developed. The lunar regolith layer consists of the low lossy regolith layer with randomly rough top and bottom interfaces, and a layer of random stone-scatterers (spatially oriented oblate spheroids are assumed) is embedded and overlays the underlying rock media. The time domain Mueller matrix solution derived from vector radiative transfer formulations contains seven scattering mechanisms of the stratified media: surface scattering from the rough top and bottom interfaces, volumetric scattering from random stone scatterers, and their multi-interactions.

Temporal characteristics and structure of the polarimetric echo profile as functional dependence on model parameters such as the layer thickness and the content of $FeO+TiO_2$, are numerically simulated, and well display an image of regolith structures. Polarimetric pulse echoes might reveal rich information of the lunar regolith layer depth and other structure properties, and demonstrate a potential new way to explore the Moon surface in future.

1. Introduction

Great advancements of the Earth terrain surface remote sensing using satellite-borne microwave passive radiometry and high resolution active synthetic aperture radar (SAR) present new potential utilities to explore the Moon and other planets. The lunar regolith layer, the uppermost layer of the Moon surface, preserves the geological history of the Moon, and the knowledge of its structure, composition and distribution might provide important information concerning the lunar geology and resources for future lunar exploration. The regolith layer thickness varies from several meters to tens of meters. Low frequency microwave can penetrate through the regolith to considerable depth.

In order to explore the potential utilities of polarimetric pulse radar sensing for Moon exploration, a theoretical model of stratified lunar regolith media with scatter inhomogeneity and rough interfaces under polarimetric radar pulse incidence is developed in our study. Temporal echoes might display the regolith structure profile. The time domain Mueller matrix solution is derived from vector radiative transfer, and is applied to numerical simulation of polarimetric radar pulse echoes from the stratified random media. The Mueller matrix solution contains seven scattering mechanisms of the stratified media: surface scattering from the rough top and bottom interfaces, respectively; volumetric scattering from random stone scatterers and their multiple interactions.

Model parameters are set according to the study of the lunar regolith structure. Temporal characteristics and structure of the polarimetric echo profile are analyzed. It displays a prominent peak due to the top boundary scattering and a complex tail due to the bottom interface and volumetric scattering of stone scarrerers. Contributions of different scattering mechanisms, i.e. surface, volumetric scattering and interactions, are analyzed, and their dependence on model parameters, such as the layer thickness and the content of $FeO+TiO_2$, are also discussed. Simulation of pulse echoes displays an image of subsurface structures. It reveals information of the regolith layer thickness, dielectric and other properties of the lunar media, and demonstrates a potential new way to explore the Moon surface in future.

2. Mueller Matrix Solution

As shown in Fig. 1, the lunar regolith layer (1) is a lossy uniform medium with thickness D, and a layer of rock scatterers (random oblate spheroids) (2) with thickness d is embedded and overlays the lunar rocky media (3). The interfaces of the regolith layer (at $z = 0$ and $z = -D$) are randomly rough and tilted surfaces.

978-1-4244-6051-9/11/$26.00 ©2011 IEEE

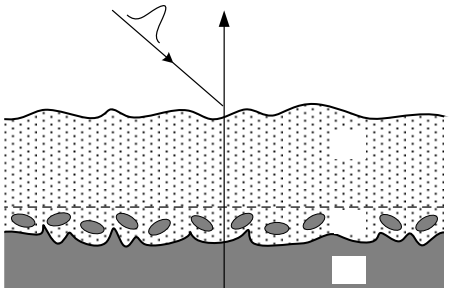

Fig. 1. A model of the lunar regolith layer.

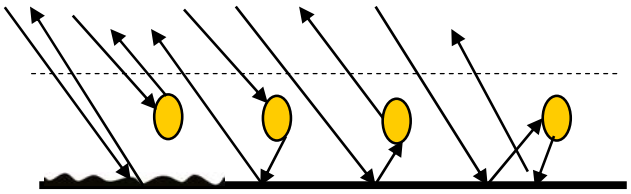

Fig. 2. Illustration of Mueller matrix.

As a polarized pulse $\mathbf{I}_0(t)$ is incident upon and through the top interface at z=0, the up-going scattered Stokes vector in the medium (1) is written as

$$\mathbf{I}(t,\Theta) = \overline{\mathbf{R}}_{01}(\Theta;\Omega_i)\mathbf{I}_0(t) + \int d\Theta' \overline{\mathbf{T}}_{10}(\Theta;\Theta') \exp(-\tau_1/\mu') \cdot \int d\Omega'' \overline{\mathbf{M}}(t-t_1',\Theta';\Omega'') \exp(-\tau_1/\mu'') \cdot \overline{\mathbf{T}}_{01}(\Omega'';\Omega_i) \cdot \mathbf{I}_0(t-t_1'-t_1'') \quad (1)$$

where the first term on the RHS is the scattering from the top rough surface, $\overline{\mathbf{R}}_{mn}, \overline{\mathbf{T}}_{mn}$ are the reflection and transmission (scattering) matrixes between the layers m and n (m,n=0,1,2). The second term is the Mueller matrix to describe the scattering and transmission of the pulse in the media 1 and 2 (including two rough interfaces at the top and bottom). The optical depth is denoted by $\tau_1 = \kappa_1(D-d)$, κ_1 is the absorption coefficient of the layer 1, $\mu = \cos\theta$, $\mu' = \cos\theta'$ and $\mu'' = \cos\theta''$, and the time delay $t_1 = (D-d)/(\mu c_0)$, and t_1' and t_1'' with respective μ', μ'' in different propagation paths, respectively. The following denotations are used for the up-going wave $\Theta = (\theta, \phi)$ and down-going wave $\Omega = (\pi - \theta, \phi)$, respectively.

The 4×4-D Mueller matrix $\overline{\mathbf{M}}$ can be simply illustrated in Fig. 2 and the following description:

$$\overline{\mathbf{M}} = a \cdot \overline{\mathbf{R}}_{23} \cdot \mathbf{I}_0 + a \cdot \overline{\mathbf{P}} \cdot \mathbf{I}_0 + a \cdot \overline{\mathbf{P}} \cdot a \cdot \overline{\mathbf{R}}_{23} \cdot a \cdot \mathbf{I}_0 + a \cdot \overline{\mathbf{R}}_{23} \cdot a \cdot \overline{\mathbf{P}} \cdot a \cdot \mathbf{I}_0 + a \cdot \overline{\mathbf{R}}_{23} \cdot a \cdot \overline{\mathbf{P}} \cdot a \cdot \overline{\mathbf{R}}_{23} \cdot a \cdot \mathbf{I}_0 \quad (2)$$

where $\overline{\mathbf{R}}_{23}$ is the scattering matrix of the bottom rough surface at $z = -D$, $\overline{\mathbf{P}}$ is the phase matrix of the stone scatterers, and a indicates propagation and is not specified herewith.

Actually, scattering and transmission can be decomposed into coherent and incoherent parts, i.e.

$$\overline{\mathbf{R}}(\Theta;\Omega_i) = \overline{\mathbf{R}}^{in}(\Theta;\Omega_i) + \overline{\mathbf{R}}^{c}(\Theta;\Omega_i) \cdot \delta(\Omega - \Omega_i), \quad \overline{\mathbf{T}}(\Theta;\Theta_i) = \overline{\mathbf{T}}^{in}(\Theta;\Theta_i) + \overline{\mathbf{T}}^{c}(\Theta;\Theta_i) \cdot \delta(\Theta - \Theta_i^+) \quad (3)$$

It can be seen that coherent scattering is dominant for large-scale surface perturbations. Because of a large-scale smoothly perturbed lunar surface and small permittivity ($\varepsilon \sim 3$) of the lunar surface, incoherent scattering of rough surfaces and stone scatters, compared with coherent scattering, is negligible at low frequencies. Thus, it is assumed that only those incoherent scattering, transmission or volumetric scattering in the specific direction described by Fig.2 are taken into account. Thus, no integral of Θ' or Θ'' is involved, and Eq. (1) is explicitly derived as Eq. (4), where $t_2 = d/(\mu c_0)$, $\tau_2 = \kappa_2 d$, the superscripts + and – are defined following the propagation directions [5]. Seven terms in the RHS of Eq. (4) can be described in Fig. 3, where the discrete scatterers are assumed small oblate spheroids with less dense distribution, and the fluctuated and straight lines of the interfaces indicate occurrence of incoherent and coherent scattering, respectively.

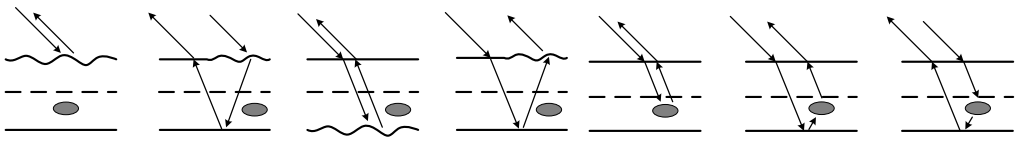

Fig. 3. Scattering mechanism of seven terms.

$$
\begin{aligned}
&\mathbf{I}(t,0^+,\Theta)=\overline{\mathbf{R}}^c_{01}(\Theta;\Omega_i)\mathbf{I}_0(t)\\
&+\overline{\mathbf{T}}^c_{10}(\Theta;\Theta^-)\cdot\overline{\mathbf{R}}^c_{23}(\Theta^-;\Omega^-)\cdot\overline{\mathbf{T}}^n_{01}(\Omega^-;\Omega_i)\,\mathrm{e}^{-2(\frac{\tau_1}{\mu^-}+\frac{\tau_2}{\mu^-})}\cdot\mathbf{I}_0(t-2t_1^--2t_2^-)\\
&+\overline{\mathbf{T}}^c_{10}(\Theta;\Theta^-)\cdot\overline{\mathbf{R}}^n_{23}(\Theta^-;\Omega_i^+)\cdot\overline{\mathbf{T}}^c_{01}(\Omega_i^+;\Omega_i)\,\mathrm{e}^{(-\frac{\tau_1}{\mu^-}-\frac{\tau_1}{\mu_i^+}-\frac{\tau_2}{\mu^-}-\frac{\tau_2}{\mu_i^+})}\cdot\mathbf{I}_0(t-t_1^--\frac{\tau_1}{\mu_i^+}-t_2^--\frac{\tau_2}{\mu_i^+})\\
&+\overline{\mathbf{T}}^n_{10}(\Theta;\Theta_i^+)\cdot\overline{\mathbf{R}}^c_{23}(\Theta_i^+;\Omega_i^+)\cdot\overline{\mathbf{T}}^c_{01}(\Omega_i^+;\Omega_i)\cdot\mathrm{e}^{-2(\frac{\tau_1}{\mu_i^+}+\frac{\tau_2}{\mu_i^+})}\cdot\mathbf{I}_0(t-2t_{1i}^+-2t_{2i}^+)\\
&+\overline{\mathbf{T}}^c_{10}(\Theta;\Theta^-)\cdot\overline{\mathbf{P}}(\Theta^-;\Omega_i^+)\cdot\overline{\mathbf{T}}^c_{01}(\Omega_i^+;\Omega_i)\frac{1}{\mu^-}\cdot\int_{-d}^{0}dz'\,\mathrm{e}^{(-\frac{\tau_1}{\mu^-}-\frac{\tau_1}{\mu^+}+\frac{\kappa_2 z'}{\mu^-}+\frac{\kappa_2 z'}{\mu^+})}\,\mathbf{I}_0\left[t+\frac{z'}{\mu^-c_0}+\frac{z'}{\mu^+c_0}-t_1^--t_{1i}^+\right]\\
&+\overline{\mathbf{T}}^c_{10}(\Theta;\Theta^-)\cdot\overline{\mathbf{R}}^c_{23}(\Theta_i^+;\Omega_i^+)\cdot\overline{\mathbf{T}}^c_{01}(\Omega_i^+;\Omega_i)\frac{1}{\mu^-}\int_{-d}^{0}dz'\,\mathrm{e}^{(-\frac{\tau_1}{\mu^-}-\frac{\tau_1}{\mu_i^+}-\frac{\tau_2}{\mu_i^+}+\frac{\kappa_2 z'}{\mu^-}-\frac{\tau_2}{\mu_i^+}-\frac{\kappa_2 z'}{\mu_i^+})}\\
&\quad\cdot\bar{\mathbf{I}}\left[t+\frac{z'}{\mu^-c_0}-\frac{d}{\mu_i^+c_0}-\frac{z'}{\mu_i^+c_0}-\frac{d}{\mu_i^+c_0}-t_1^--t_{1i}^+\right]\\
&+\overline{\mathbf{T}}^c_{10}(\Theta;\Theta^-)\cdot\overline{\mathbf{R}}^c_{23}(\Theta^-;\Omega^-)\cdot\overline{\mathbf{P}}(\Omega^-;\Omega_i^+)\cdot\overline{\mathbf{T}}^c_{01}(\Omega_i^+;\Omega_i)\frac{1}{\mu^-}\int_{-d}^{0}dz'\,\mathrm{e}^{(-\frac{\tau_1}{\mu^-}-\frac{\tau_1}{\mu_i^+}-\frac{\tau_2}{\mu^-}-\frac{\tau_2}{\mu_i^+}+\frac{\kappa_2 z'}{\mu^-}-\frac{\kappa_2 z'}{\mu_i^+})}\\
&\quad\cdot\mathbf{I}_0\left[t-\frac{d}{\mu^-c_0}-\frac{d}{\mu^-c_0}-\frac{z'}{\mu^-c_0}+\frac{z'}{\mu_i^+c_0}-t_1^--t_{1i}^+\right]
\end{aligned}
\tag{4}
$$

To take account of large scale perturbations of the tilted lunar surface, the Mueller matrix $\overline{\mathbf{M}}_g$ in principal coordinates (x_g, y_g, z_g) can be obtained by orientation transformation of local $\overline{\mathbf{M}}$ as

$$
\overline{\mathbf{M}}_g=\overline{\mathbf{U}}(\Delta_s)\cdot\overline{\mathbf{M}}\cdot\overline{\mathbf{U}}(\Delta_i) \tag{5}
$$

3. Numerical Simulation of Radar Echoes Image

Low frequency 1.4 GHz (L band) sensing is assumed in this paper for predicted full penetration through the regolith layer. The incident Gaussian pulse of plane wave is given as

$$
I_0(t)=\exp[-b^2(t-T_0)^2] \tag{6}
$$

where $b=\sqrt{\ln 2}/T_w$, $2T_w$ is the half-power width (12 ns), and T_0 is the time of the pulse echo peak (18 ns), and $B_w=2\ln 2/T_w=231\mathrm{MHz}$. The parameters are designed, based on the Moon topography, as follows: $D=500$ cm, $d=150$ cm, the semi-axes of oblate spheroid stone 2.5 cm and 1 cm, its fractional volume 0.02 and spatial orientation over $\beta\in(0^\circ,60^\circ)$, $\gamma\in(0^\circ,360^\circ)$. The dielectric permittivity of the regolith layer is 3+0.01i (corresponding to the FeO+TiO_2 content 6%), and both the dielectric permittivity of the stone scatterers and underlying rock media are chosen as 8+0.5i. The rough interfaces are Gaussian with the roughness variance and correlation length, 4 cm and 20 cm for the top interface, and 2 cm, 40 cm for the bottom interface, respectively. The incident angle in all examples is $\theta_i=30^\circ$.

Polarized back- and bistatic scattering contributed by seven terms described in Eq. (4) can be obtained. It is expected that if there exist non-uniform and random stratified structures in the regolith layer (1), random fluctuations and multi-reflections can happen during the propagation time, e.g. 0-25ns. Also, if the structure of the layered media is anisotropic, different polarized echoes will display more significantly different responses and might reveal more information about the media.

The regolith results from continuous impacts of large and small meteoroids during the long history of Moon geology, and its average thickness is about 4-5 m for Maria and about 10-15 m for highlands. In general, the regolith layer thickness correlates well with the lunar surface age: the greater the age, the thicker the regolith deposit. We propose to construct the lunar regolith layer thickness proportional to the altitude in the lunar DEM as a tentatively chosen distribution.

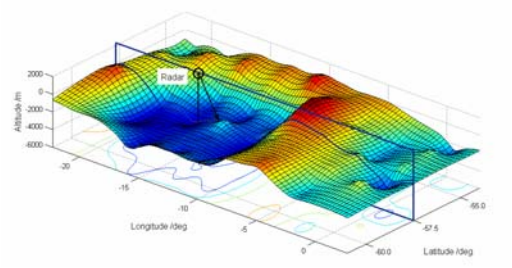

Fig. 4. Geometry of the image area.

Simulation of the pulse echoes can show stratified structures of the lunar regolith media. In radar probing with high resolution, the echoes from aligned pixels can compose an image, as illustrated in Fig. 4.

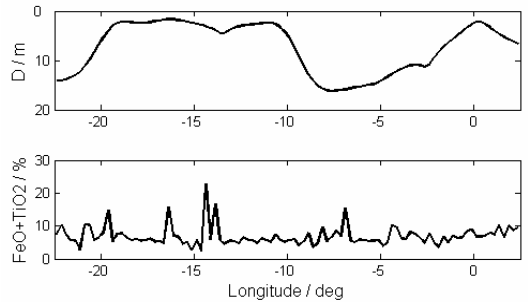

Fig. 5 Parameters of the lunar surface

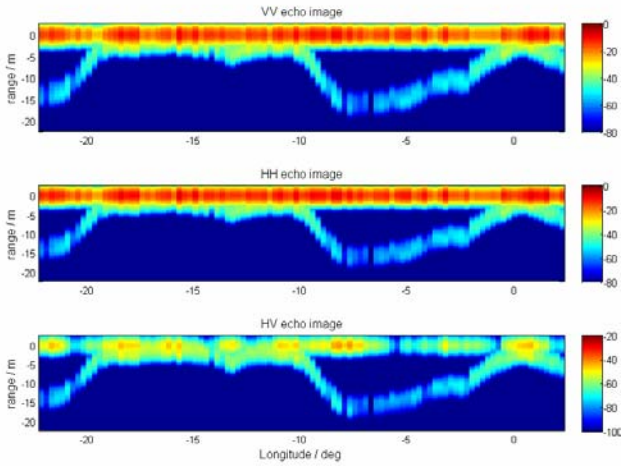

Fig. 6. Image of polarimetric pulse echoes.

As an example, the parameters of the assumed DEM, regolith layer thickness, $FeO+TiO_2$ content at the lunar location along the latitude S57.5° from the longitude W22.5° to E2.5° (at Clavius) are chosen, as shown in Figs. 5(a,b), and surface roughness are assumed to be of the order of 10% random fluctuation.

Figs. 6(a,b,c) show the image of co-polarized *hh, vv* and cross-polarized *hv* pulse echoes, respectively. In Figs. 6(a,b,c), each pixel is of the resolution of about 4.1 km. The profile of the regolith layer depth and the stone scatter layer can be identified. More information can be retrieved from fully polarimetric pulse echoes.

Some other applications can be further demonstrated.

References

[1] Y.Q. Jin, *Theory and Approach of Information Retrievals from Electromag-netic Scattering and Remote Sensing*. Berlin Heidelberg New York: Springer, 2005.

[2] Y.Q. Jin and F. Chen, "Scattering Simulation for Inhomogeneous Layered Canopy and Random Targets Beneath Canopies by Using the Mueller Matrix Solution of the Pulse Radiative Transfer", *Radio Science*, 38(6): 1107-1116, 2003.

[3] Y.Q. Jin, F. Chen and M. Chang, "Retrievals of Underlying Surface Roughness and Moisture for Stratified Vegetation Canopy Using Polarized Pulse Echoes in the Specular Direction," *IEEE Transactions on Geoscience and Remote Sensing*, 42(2): 426-433, 2004.

[4] W. Fa and Y.Q. Jin, "Simulation of Brightness Temperature of Lunar Surface and Inversion of the Regolith Layer Thickness", *Journal of Geophysical Research-Planet*, 112, E05003, doi:10.1029/2006JE00 2751: 1-13, 2007.

[5] Y.Q. Jin, F. Xu and W. Fa, "Numerical Simulation of Polarimetric Radar Pulse Echoes from Lunar Regolith Layer with Scatter Inhomogeneity and Rough Iterfaces", *Radio Science*, 42, RS3007, doi: 10.1029/RS2006 003523: 1-10, 2007.